Design and test of an adaptive self-excited/forced mode intelligent vibrating subsoiler

Mingzhuo Guo[1], Wen Yang[1], Chengliang Zhang[1,2], Xiaosong Sun[1], Junxiang Zhao[1], Baofeng Wang[1], Tianyi Lan[3], Guohui Feng[3*], Jiale Zhao[1,3*]

(1. *College of Biological and Agricultural Engineering, Jilin University, Changchun 130022, China*;
2. *Harbin Academy of Agricultural Sciences, Harbin 150029, China*;
3. *National Key Laboratory of Smart Farm Technologies and Systems, Harbin 150030, China*)

Abstract: Subsoiling is an effective tillage technique for alleviating soil compaction, but the high traction resistance encountered at deeper working depths constrains its widespread application. To address this issue, a self-excited and forced intelligent vibrating subsoiler was developed. The subsoiler is equipped with a compound vibration mechanism that can adaptively switch between self-excited vibration and forced vibration modes based on real-time monitoring of soil resistance. Field experiments were conducted to evaluate the performance of the self-excited and forced vibrating subsoiling (SEFV). These experiments compared its performance with conventional subsoiling (CS) and self-excited vibrating subsoiling (SEV) at different working depths (35-45 cm) and forward speeds (2 and 4 km/h). The results showed that at 2 km/h, SEFV operated in self-excited vibration mode and reduced traction resistance by 12.4%-13.1% compared to CS, with no significant difference from SEV. At 4 km/h, the resistance reduction effect of SEFV became more pronounced with increasing depth. At 45 cm depth, SEFV reduced traction resistance by 9.9% and 18.9% compared to SEV and CS, respectively, as it switched to forced vibration mode to overcome the high soil resistance. SEFV also maintained high subsoiling depth stability (>90%) at both speeds and all depths tested, demonstrating its advantage over SEV under high resistance conditions. The intelligent control system based on resistance feedback enabled the SEFV to automatically adapt to variable soil conditions and optimize its vibration behavior for improved subsoiling performance and energy efficiency. This study provides new insights into the design of adaptive vibrating subsoilers for enhanced tillage operations.

Keywords: vibrating subsoiler, self-excited vibration, forced vibration, adaptive control, vibration mode switching
DOI: 10.25165/j.ijabe.20251804.9420

Citation: Guo M Z, Yang W, Zhang C L, Sun X S, Zhao J X, Wang B F, et al. Design and test of an adaptive self-excited/forced mode intelligent vibrating subsoiler. Int J Agric & Biol Eng, 2025; 18(4): 101–109.

1 Introduction

Subsoiling, as an important conservation tillage technique, can effectively alleviate soil compaction issues, increase crop yields and economic returns, and has been widely applied worldwide[1]. However, during the subsoiling process, the subsoiling components need to work in the 25-40 cm soil layer, where the resistance encountered is much greater than in other surface tillage operations. As the working depth increases, the resistance grows exponentially, making subsoiling one of the most energy-consuming operations in soil tillage. To a certain extent, this constrains the promotion and application of subsoiling technology[2,3]. Therefore, reducing the traction resistance of subsoiling machinery is crucial, and is of great significance for energy and cost savings, as well as promoting the widespread application of subsoiling operations[4].

Vibrating subsoiling technology is currently one of the most effective methods for reducing resistance in subsoiling operations. The basic principle is to attach vibrating elements to the subsoiling components, causing the subsoiler to vibrate in the soil, break up soil clods, and reduce soil resistance[5-7]. According to the different types of vibration sources, vibrating subsoiling can be divided into two types: self-excited and forced. Self-excited vibration sets elastic elements between the subsoiler and the frame, utilizing changes in soil resistance to excite vibration[8-10]. For example, Wang et al.[11,12] designed a self-excited vibrating subsoiling method using a hydraulic cylinder as the excitation source, which can achieve rapid adjustment of hydraulic cylinder pressure. To reduce subsoiling resistance and improve subsoiling quality, Cui et al.[13] designed a vibrating subsoiler powered by the tractor's output shaft, with a vibrating mechanism composed of an eccentric shaft and a cross connector, significantly reducing the traction resistance by 9.09%. Zhang et al.[14] designed a forced vibrating subsoiling mechanism based on a crank-rocker mechanism, reducing the traction force by about 14% in vibration mode, while fuel consumption increased by 22%. Wang et al.[15] designed a staggered vibrating subsoiling mechanism based on a gear reducer, greatly improving soil crushing

Received date: 2024-10-12 **Accepted date:** 2025-05-13
Biographies: Mingzhuo Guo, PhD, Associate Professor, research interest: bionic intelligent agricultural machinery, Email: gmz@jlu.edu.cn; **Wen Yang**, Research Assistant, research interest: intelligent agricultural machinery, Email: yangwen1822@163.com; **Chengliang Zhang**, PhD, research interest: intelligent ploughing machinery and equipment design, Email: obama1@163.com; **Xiaosong Sun**, MS, research interest: sensor fusion and control systems for precision agriculture equipment, Email: sunxs22@mails.jlu.edu.cn; **Junxiang Zhao**, Research Assistant, research interest: soil dynamics and optimization of tillage machinery, Email: zhaojx9922@mails.jlu.edu.cn; **Baofeng Wang**, Research Assistant, research interest: agricultural machinery electrification, Email: wangbf1822@mails.jlu.edu.cn; **Tianyi Lan**, Researcher, research interest: agricultural intelligence and informatization, Email: lantianyi@chinabdh.com.
***Corresponding author: Guohui Feng**, Associate Professor, research interest: intelligent agricultural machinery. National Key Laboratory of Smart Farm Technologies and Systems, Harbin 150030, China. Tel: +86-15045790771, Email: fengguohui@chinabdh.com; **Jiale Zhao**, PhD, Professor, research interest: bionic intelligent agricultural machinery. Jilin University, Changchun 130022, China. Tel: +86-18843165417, Email: zhaojl@jlu.edu.cn.

ability while reducing wheel slippage.

Existing research shows that self-excited vibrating subsoilers can meet the resistance reduction requirements under most soil conditions. However, the presence of aggregates and pore structures in the soil can easily lead to uneven subsoiling traction resistance, especially when the subsoiling depth exceeds 40 cm. Due to the significant increase in soil resistance, self-excited vibration is limited by the vibration threshold of the elastic elements, making it difficult to effectively break up over-hard or over-sticky soil layers, and may even lead to vibration failure and inability to work normally[16-18]. Forced vibration, on the other hand, is equipped with a dedicated excitation device that can provide stronger vibration force and has stronger soil crushing and surface straw cutting capabilities, making it more suitable for subsoiling operations under soil conditions with excessive resistance. However, forced vibration requires additional energy input to drive the excitation device, which may cause energy waste under normal soil conditions[19].

To address the above issues, this study proposes an intelligent vibrating subsoiler that can adaptively switch between vibration modes. This machine is equipped with a tillage resistance recognition device and a vibration mode switching mechanism, which can automatically switch between self-excited vibration and forced vibration according to the magnitude of soil resistance. Under normal soil conditions with lower resistance, self-excited vibration is used, while under complex soil conditions with higher resistance, it switches to forced vibration. This adaptive vibration mode switching strategy not only ensures stable operation under various soil conditions but also avoids energy waste caused by continuous forced vibration, achieving a balance between resistance reduction and energy saving. Field experiments of this subsoiler were conducted at the Heilongjiang Academy of Agricultural Sciences, verifying its good working performance and providing new ideas and technical support for the design optimization of vibrating subsoiling machinery.

2 Materials and methods

2.1 Overall machine design

The overall structure of the vibrating subsoiler, as shown in Figure 1, mainly consists of key components such as the main frame, vibrating subsoiling units, tension sensor, power source, control system, and ground wheels. The main frame is the skeleton of the entire machine, welded from high-strength steel materials, with high rigidity and strength to reliably connect and support various components. The vibrating subsoiling unit is the core working component of this machine, with a total of three sets arranged equidistantly across the main frame at a spacing of 650 mm, enabling simultaneous three-row operation. Each subsoiling unit consists of a subsoiling blade, spring vibration mechanism, and eccentric vibration motor. The subsoiling blade is made of special materials with high hardness and wear resistance, capable of effectively breaking up soil while having strong abrasion resistance and long service life. The spring vibration mechanism consists of a set of tension and compression springs, responsible for the self-excited vibration of the subsoiling mechanism, while the eccentric vibration motor provides forced vibration. The two cooperate to adaptively adjust the vibration mode according to changes in soil resistance. The working depth of the subsoiling blade can be adjusted in the range of 300-500 mm through an adjustment mechanism to meet different tillage depth requirements.

The tension sensor is installed between the subsoiling unit and the frame to monitor the changes in traction resistance during the subsoiling process in real-time, providing a basis for adaptive adjustment of the vibration mode. The power source can be a gasoline generator or a battery pack. This machine adopts a more economical gasoline generator to power the eccentric vibration motor. The control system is the “brain” of this machine, using an STM32 controller as the control center. The control system receives and processes signals from the tension sensor. Based on preset control strategies, it automatically adjusts power output and vibration mode to achieve adaptive control of the entire machine. The ground wheels are installed at the rear of the frame and work in coordination with the subsoiling blade to precisely control subsoiling depth and ensure the stability of operation quality. In summary, the various components of this vibrating subsoiler cooperate to form an efficient and reliable integrated system that can adaptively adjust the vibration mode according to changes in soil resistance, fully leveraging the advantages of vibrating subsoiling to improve subsoiling quality and operation efficiency.

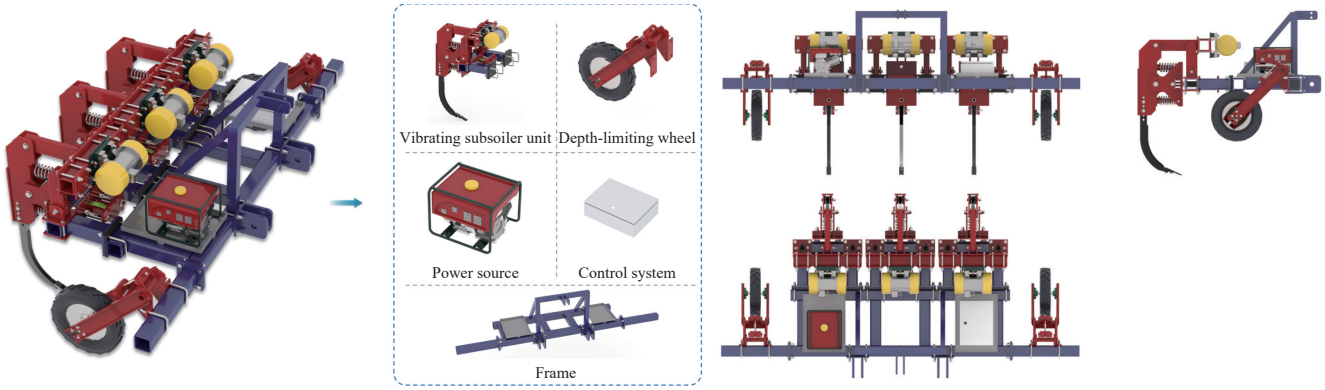

a. Overall structure and main components b. Three-view drawing of the overall structure

Figure 1 Structure of the overall machine

2.2 Working mechanism

The working principle of this vibrating subsoiler is to break up the soil and achieve subsoiling through the interaction between the vibrating subsoiling unit and the soil. During actual operation, this machine can adaptively switch between two working modes, self-excited vibration and forced vibration, to adapt to different soil conditions. When the soil resistance is small, the subsoiling unit undergoes self-excited vibration under the action of the spring vibration mechanism (Figure 2a). The vibrating arm deforms when the subsoiling blade encounters soil resistance, storing elastic potential energy. When the subsoiler breaks through the soil resistance, the vibrating arm quickly returns to its original position

under the action of the spring, releasing the stored elastic potential energy and driving the subsoiler to vibrate and break up the soil. This self-excited vibration mode does not require additional energy input and utilizes soil resistance to generate vibration, resulting in high energy utilization efficiency. When encountering soil with greater resistance, relying solely on self-excited vibration may be difficult to meet subsoiling requirements. At this point, the tension sensor detects that the traction resistance exceeds the preset threshold and transmits the signal to the control system. The control system immediately starts the eccentric vibration motor to apply additional vibration force to the subsoiling unit, generating forced vibration (Figure 2b). Superimposing forced vibration on the basis of self-excited vibration can effectively overcome greater soil resistance and ensure subsoiling effects.

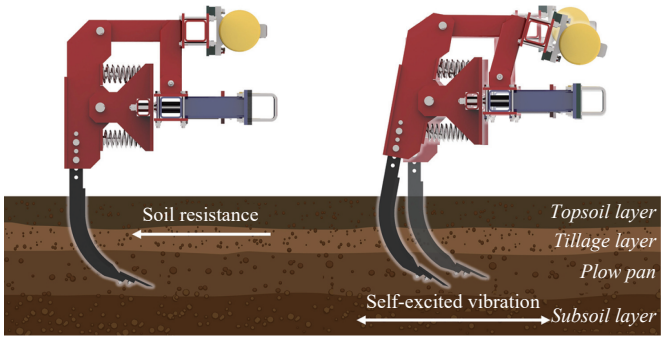

a. Self-excited vibration mode

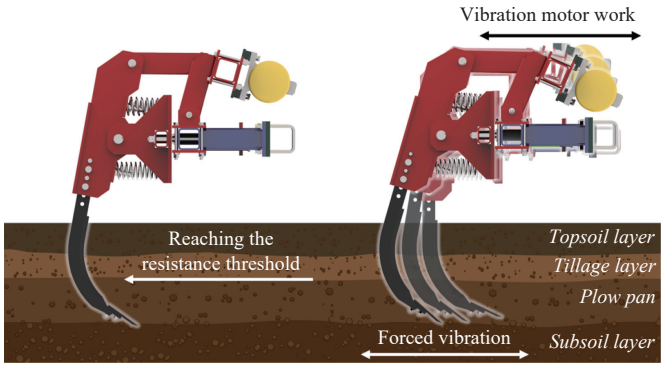

b. Forced vibration mode

Figure 2 Schematic diagram of self-excited and forced vibration subsoiling modes

It is worth mentioning that this vibrating subsoiler is equipped with an adaptive control system based on resistance feedback. During operation, the tension sensor continuously monitors changes in traction resistance and transmits the resistance signal to the control center in real-time. The control center determines whether to start forced vibration based on the preset resistance threshold. When the resistance is below the threshold, the self-excited vibration mode is maintained; when the resistance exceeds the threshold, the forced vibration mode is activated. By monitoring changes in soil resistance in real time and automatically adjusting the vibration mode, the advantages of vibrating subsoiling can be fully leveraged to improve subsoiling quality while reducing energy consumption and increasing operating efficiency. In addition, thanks to the independent subsoiling unit design, this machine can also adjust the vibration mode for each subsoiling unit separately according to the spatial variability of soil properties, achieving more refined adaptive control. For example, for fields with uneven soil resistance distribution, self-excited vibration can be used in areas with lower resistance, while forced vibration can be used in areas with higher resistance, fully adapting to changes in soil conditions and improving subsoiling effects and operation quality.

In summary, by switching between self-excited vibration and forced vibration modes, combined with an adaptive control strategy based on resistance feedback, this vibrating subsoiler can automatically adjust vibration behavior according to changes in soil resistance. While improving subsoiling quality and operation efficiency, it also optimizes energy consumption, exhibiting good adaptability and practicality.

2.3 The key component design

2.3.1 Design of self-excited and forced compound vibration mechanism

The self-excited and forced subsoiling mechanism consists of two parts based on the different working states: self-excited vibration and forced vibration. The detailed structure of this mechanism is shown in Figure 3. The mounting bracket, connecting rod, connecting bracket, and connecting rod fixing plate together form a four-bar linkage mechanism, allowing the subsoiler shank to vibrate within a certain range. The subsoiler shank is fixed to the mounting bracket with bolts after installing damping pads on both sides, and the mounting bracket is connected to the connecting rod fixing plate through positioning pins, allowing rotation around the positioning pin axis. During the vibrating subsoiling process, the soil continuously exerts thrust on the subsoiler shank. This mechanism achieves vibration drag reduction through two cylindrical helical springs. After the spring installation position is limited by the spring positioning pins on the mounting bracket, it can be clearly seen that the upper spring is always under compression and the lower spring is always under tension, so the spring parameters need to be calculated.

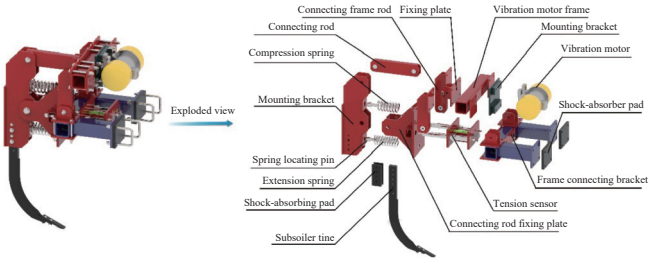

Figure 3 Schematic diagram of self-excited and forced compound vibration subsoiling mechanism

The parameters of the upper and lower springs are calculated according to the mechanical design manual. Based on literature research, the maximum subsoiling resistance value of 4000 N is initially selected for calculation. Since the compression spring is located above the vibration device and forms a lever through the rotation center, the tension spring and compression spring are equidistant from the lever center, so they can be considered to work under the same tension or compression scale. The compression spring is designed, and the combined force of the two springs achieves vibrating subsoiling, with each spring operating under an average condition of 1000-1500 N. First, the compression spring is designed. During installation, the spring undergoes pre-tightening, so the minimum load F_{min}=100 N and the maximum load F_{max}= 2000 N are initially estimated. According to the vibration motion mode of the subsoiler shank, it can be known that the spring deformation can be constructed with a similar stress analysis to the

subsoiler shank motion state, so the spring deformation can be estimated based on the horizontal displacement of the subsoiler shank.

2.3.2 Design of self-excited spring parameters

As seen in Figure 4, the compression and tension springs are symmetrically arranged around the central pivot. This symmetrical arrangement implies that the magnitude of compression (l_c) equals the magnitude of tension (l_t) for a given deflection angle α[20,21]. The force and dimensional relationships can be analyzed based on this structure, approximating the geometry with similar triangles (the relation is $l = \sin\alpha$). The design calculations for the required spring characteristics are based on Equation (1):

$$\begin{cases} K = \dfrac{4C-1}{4C-4} + \dfrac{0.615}{C} \\ d \geq 1.6\sqrt{\dfrac{F_{\max} KC}{[\tau]}} \end{cases} \quad (1)$$

where, K is the curvature coefficient, C is the winding ratio (defined as $C = D/d$, where D is the mean coil diameter), $[\tau]$ represents the allowable stress of the chosen spring material, and G is the shear modulus of the material. Based on the dimensional structure and standard design rules found in mechanical design manuals, the springs are classified as Class II springs. The selected material is 60Si2MnA, which possesses an allowable stress $[\tau]$ = 640 MPa and a shear modulus $G = 8\times10^4$ MPa. After substituting the relevant coefficients and checking the table, the standard diameter is selected. The diameter is appropriately increased within a suitable range to prevent sudden load changes. Finally, d=8 mm is determined, and the number of spring coils is determined according to Equation (2)[22]:

$$n = \frac{Gd^4}{8D_2^3 k} \quad (2)$$

The calculated parameters are substituted to obtain n=9.82, which is rounded to n=10 for the number of spring coils. Since the upper spring is under compression, according to the manual requirements, the number of support coils at both ends is one turn each, so the total number of coils is n=12. The final calculated spring parameters are listed in Table 1.

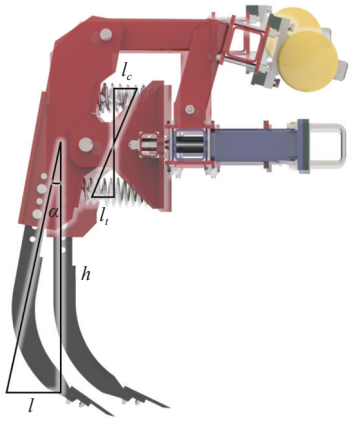

Note: α represents the deflection angle of the subsoiler shank, which is equivalent to the deflection angle of the single-sided deformation process of the springs. The length of the subsoiler shank is denoted by h. The horizontal displacement of the subsoiler shank tip after deflection is represented by l. Corresponding to this deflection, l_c signifies the compression amount of the upper spring, and l_t signifies the tension (elongation) amount of the lower spring.

Figure 4 Schematic diagram of spring deformation

Table 1 Spring parameters

	Compression spring (Upper pressure)	Tension spring (Lower tension)
Material	60Si2MnA	
winding ratio C	7	
Curvature coefficient K	1.21	
Stiffness/N·mm^{-1}	23.75	
Mean diameter D_2/mm	56	70
Outer diameter D/mm	64	80
Spring wire diameter d/mm	8	10
Number of active coils n	12	10
Pitch p/mm	16	10
Free height H_0/mm	204	100

2.3.3 Intelligent circuit design

The forced vibration mode of the self-excited and forced compound vibration mechanism is completed by the four key components shown in Figure 5, which together form an adaptive control system. The specific implementation process is shown in Figure 5. First, the S-type tension sensor measures the subsoiling resistance of the subsoiling unit. When it reaches a set high resistance threshold, the control system makes a judgment and starts the power source to drive the vibration motor, applying an even stronger vibration force to the mechanism on top of the self-excited vibration, further crushing the high-resistance soil and further reducing the subsoiling resistance.

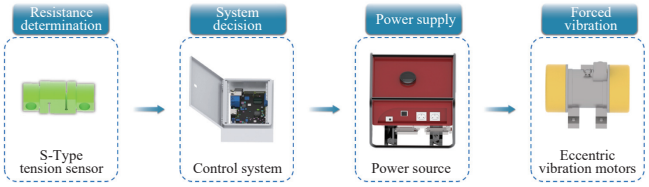

Figure 5 Schematic diagram of forced subsoiling principle

To realize the adaptive switching of vibration modes for the vibrating subsoiler, this study designed an intelligent control circuit system based on the STM32-S3 microcontroller. The core control component of this circuit is the STM32-S3 microcontroller, which has rich peripheral interfaces and strong data processing capabilities, meeting the system's requirements for real-time performance and reliability[23]. The hardware part of the intelligent control circuit system, the schematic of which is shown in Figure 6, mainly includes the power supply circuit, tension sensor signal output circuit, STM32-S3-based control circuit, etc. The power supply circuit adopts an AC-DC step-down circuit to convert the 220 V voltage output by the gasoline generator into three voltage levels of 12 V, 5 V, and 3.3 V to power the tension sensor and microcontroller, respectively. The tension sensor uses a strain-type S-shaped sensor with a measurement range of 4 kN, selected to adequately cover the expected maximum subsoiling resistance encountered during experiments. These sensors typically operate based on the strain gauge principle, where applied force causes deformation that changes the electrical resistance of gauges bonded to the sensor body. This change in resistance is then converted into an electrical signal proportional to the force. They generally offer good linearity and a typical accuracy (e.g., ±0.05% of full scale), which provides sufficient resolution for detecting the resistance variations required to trigger the adaptive control logic in this study. The output signal of the tension sensor directly communicates through the GPIO port of the microcontroller, transmitting the

tension value to the microcontroller in real time. The control circuit is centered on the STM32-S3 microcontroller, with extended crystal oscillator circuit, reset circuit, indicator lights, etc., forming the main body of the control system. The motor drive circuit uses a frequency converter to control the speed of the eccentric motor. The control signal is sent by the STM32-S3 and the motor speed command is transmitted to the frequency converter via RS485, thereby changing the rotation speed of the motor[24].

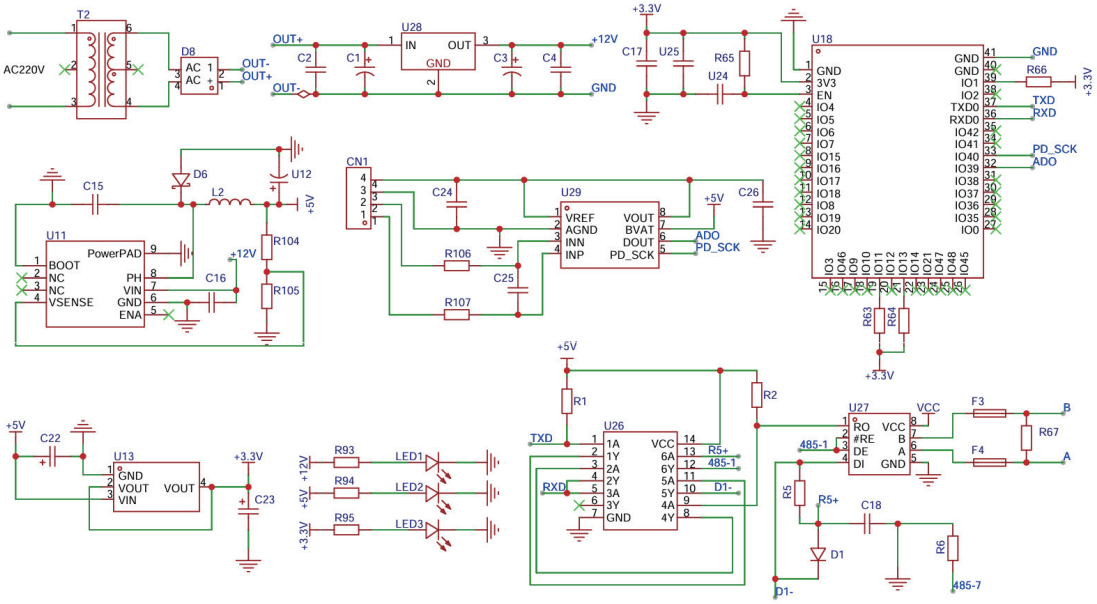

Figure 6 Hardware circuit diagram

The main program of the control system is developed using Visual Studio Code software, based on the ESP-IDF framework, and mainly includes modules such as system initialization, sensor data acquisition, and adaptive threshold control algorithm. After the system is powered on, it first performs initialization to complete the configuration of various peripherals. Next, the collected tension sensor data is filtered through a low-pass filtering algorithm and finally converted into traction resistance values according to the conversion formula. The adaptive threshold control algorithm judges the current soil resistance state based on the real-time resistance value F fed back by the tension sensor. When F is less than the set threshold T_1, the motor does not rotate, and only self-excited vibration is used. When the condition where F continuously exceeds T_1 persists for a duration of 0.5 s or more, the frequency converter starts the motor. This 0.5 s time threshold is implemented as a filter to prevent unnecessary mode switching triggered by transient resistance spikes, ensuring the system responds only to sustained high-resistance conditions. While there is a minimal inherent processing delay within the microcontroller and communication latency with the frequency converter (typically in the order of millis), this is considered negligible compared to 0.5 s logical delay designed to enhance control stability by avoiding rapid oscillations between modes. When F is greater than T_1 but less than T_2, it maintains a lower rotation speed S_1 and superimposes a weaker forced vibration. When F continues to increase beyond T_2, the motor speed is increased to S_2, thereby superimposing a stronger forced vibration. During the forward movement of the machine, the microcontroller will detect the resistance value emitted by the tension sensor in real time. When F is less than T_2, the motor will promptly adjust to speed S_1 for weaker forced vibration. When F is lower than T_1, the motor will stop rotating and perform self-excited vibration. The thresholds T_1, T_2 and speeds S_1, S_2 can be flexibly set according to soil characteristics and operation requirements to meet different working scenarios. The software flowchart of the control system is presented in Figure 7.

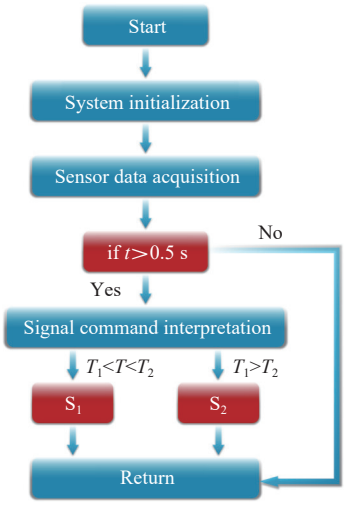

Figure 7 Software flowchart

3 Tests and methods

3.1 Test conditions

The experiments were conducted from November 2 to November 5, 2023 at the experimental base of the Heilongjiang Academy of Agricultural Sciences. The base is located in Harbin City, Heilongjiang Province (126°38′E, 45°45′N), with a temperate continental monsoon climate. The annual average temperature is 3.5°C, the accumulated temperature ≥10°C is 2300°C-2500°C, the annual precipitation is 500-600 mm, and the frost-free period is 135-140 d. The soil type in the test field is black soil, with a uniform soil texture and medium-high organic matter content. The physical parameters of the soil at different depths are listed in Table 2. The field had been under a continuous maize cropping system for the previous five years and was selected for its relatively uniform soil

conditions across the experimental area.

The tested crop was the locally dominant maize variety "Hengyu 1", with a sowing date of May 20 and a harvest date of September 25. The planting density was 60 000 plants per hectare, and the fertilizer application rate was 150 kg of pure nitrogen, 75 kg of P_2O_5, and 60 kg of K_2O per hectare. Except for the subsoiling treatment, other field management measures were the same and carried out according to local field production practices. The main instruments and equipment used in the experiment included: Dongfanghong-1804 tractor, Spectrum TDR-300 soil moisture rapid tester, RKT-5 soil hardness tester, etc. The machine during the field test is shown in Figure 8.

Figure 8 Machine field test

Table 2 Soil parameters

Soil depth/cm	Moisture content/%	Compaction/kPa	Soil density/g·cm^{-3}
25-30	21	1055	1.47
30-35	21.5	1201	1.5
35-40	21.7	1447	1.52
40-45	22	1642	1.59

3.2 Test methods

The experiment adopted a randomized complete block design with three treatments and three replicates. The plot area was 300 m^2. The three treatments compared, as defined in Table 3, were: conventional subsoiling (CS), self-excited vibrating subsoiling (SEV), and the self-excited and forced vibrating subsoiling (SEFV). The assignment of these treatments to plots within each replicate block was randomized. The working depths were 35 cm, 40 cm, and 45 cm. SEFV used the vibrating subsoiler designed in this study; CS used the 1SZL-7 subsoiling machine, which has a traditional rigid connection structure between the subsoiler blade and frame; SEV used the 1SFZ-3 self-excited vibrating subsoiler previously developed by the research team, which has the same self-excited vibration unit as this study, but without the forced vibration components installed. The subsoiling resistance was collected using LZ-LS7 column-type tension-compression force sensors mounted on the front of each subsoiling unit. The traction resistance of a single subsoiler blade can be obtained by dividing the total resistance by the number of subsoiling units.

Table 3 Operation modes

Mode	Machine type
CS	Conventional subsoiling
SEV	Self-excited vibrating subsoiling
SEFV	Self-excited and forced compound vibration mechanism

The experiment simulated two common tractor operating speeds for subsoiling: 2 km/h and 4 km/h. Considering that relevant studies[16-18] suggest the performance limitations of purely self-excited vibration systems under high soil resistance (typically above 3-4 kN), and based on our preliminary experiments, the specific threshold value (T_1) for switching to forced vibration was set at 3500 N. Therefore, the SEFV was configured to operate in its default self-excited vibration mode when the measured traction resistance was below 3500 N, automatically switching to the forced vibration mode when the resistance exceeded this threshold for a duration of 0.5 s. Traction resistance data were continuously acquired for 20 s after the working state stabilized, using sensors with a recording frequency of 2 Hz (corresponding to a 0.5 s interval).

Regarding the vibration frequency during the forced vibration phase of the SEFV, while the control system is capable of adjusting motor speed to vary the frequency/intensity, the primary objective of this specific field experiment was to validate the adaptive switching mechanism based on the T_1 threshold. Therefore, a fixed motor speed setting (corresponding to a specific forced vibration frequency/intensity) was used whenever the forced mode was activated. Optimization of the forced vibration frequency range or the second threshold (T_2) was not included in the scope of these trials and remains an area for future investigation.

The measurement of subsoiling depth was performed according to the qualification standards in NY/T 741-2003 "Operation Quality of Subsoiling and Stubble Cleaning Machinery". After subsoiling operation, 30 sampling points were randomly selected along the advancing direction of the machine in a single ridge operation area. The soil after subsoiling was dug open, and a steel ruler was inserted into the deepest part of the soil at the sampling point to measure and record the depth. The subsoiling depth stability was calculated according to Equation (3), with stability greater than 80% considered as qualified.

$$\begin{cases} a = \dfrac{\sum_{i=1}^{n} a_i}{n} \\ S = \sqrt{\dfrac{\sum_{i=1}^{n} (a_i - a)^2}{n-1}} \\ V = \dfrac{S}{a} \times 100\% \\ U = 1 - V \end{cases} \tag{3}$$

where, a is the average subsoiling depth, cm; a_i is the subsoiling depth value at the i-th point, cm; n is the number of sampling points; S is the standard deviation of subsoiling depth; V is the coefficient of variation of subsoiling depth; and U is the stability coefficient of subsoiling depth.

3.3 Statistical analysis

Analysis of variance (ANOVA) was conducted using statistical software (IBM SPSS Statistics 21, IBM, USA) to examine the effects of the experimental factors (CS, SEV, and SEFV) on subsoiling depth and traction resistance at different forward speeds. Means of measured variables were compared using the Least Significant Difference (LSD) test. Statistical significance was evaluated at $p < 0.05$.

4 Results and discussion

4.1 Traction resistance

The test results of traction resistance are shown in Figure 9. According to the analysis of Figures 9a-9c, at the slow working speed of 2 km/h, the traction resistance did not reach the set threshold of the compound vibrating subsoiler at all working depths.

At a depth of 35 cm, the average traction resistance of CS, SEV, and SEFV was 2743 N, 2357 N, and 2395 N, respectively. At a depth of 40 cm, the average traction resistance of CS, SEV, and SEFV was 3304 N, 2934 N, and 2895 N, respectively. At a depth of 45 cm, the average traction resistance of CS, SEV, and SEFV was 3820 N, 3322 N, and 3292 N, respectively. It can be seen that because forced vibration was not working and all were in self-excited vibration mode, there was no significant difference in traction resistance between SEV and SEFV (difference <5%). Since the self-excited vibration mode improved the soil breaking ability of the subsoiler blade, at 2 km/h and the three working depths, the SEFV designed in this study had no significant difference from SEV, but the resistance was reduced by 12.7%, 12.4%, and 13.1%, respectively, compared to CS. This lack of significant difference between SEV and SEFV confirms that, at the lower speed of 2 km/h, the traction resistance consistently remained below the 3500 N threshold required to activate the forced vibration mode in the SEFV system across all tested depths. Consequently, the SEFV operated solely in its self-excited vibration mode under these conditions, mirroring the behavior of the SEV.

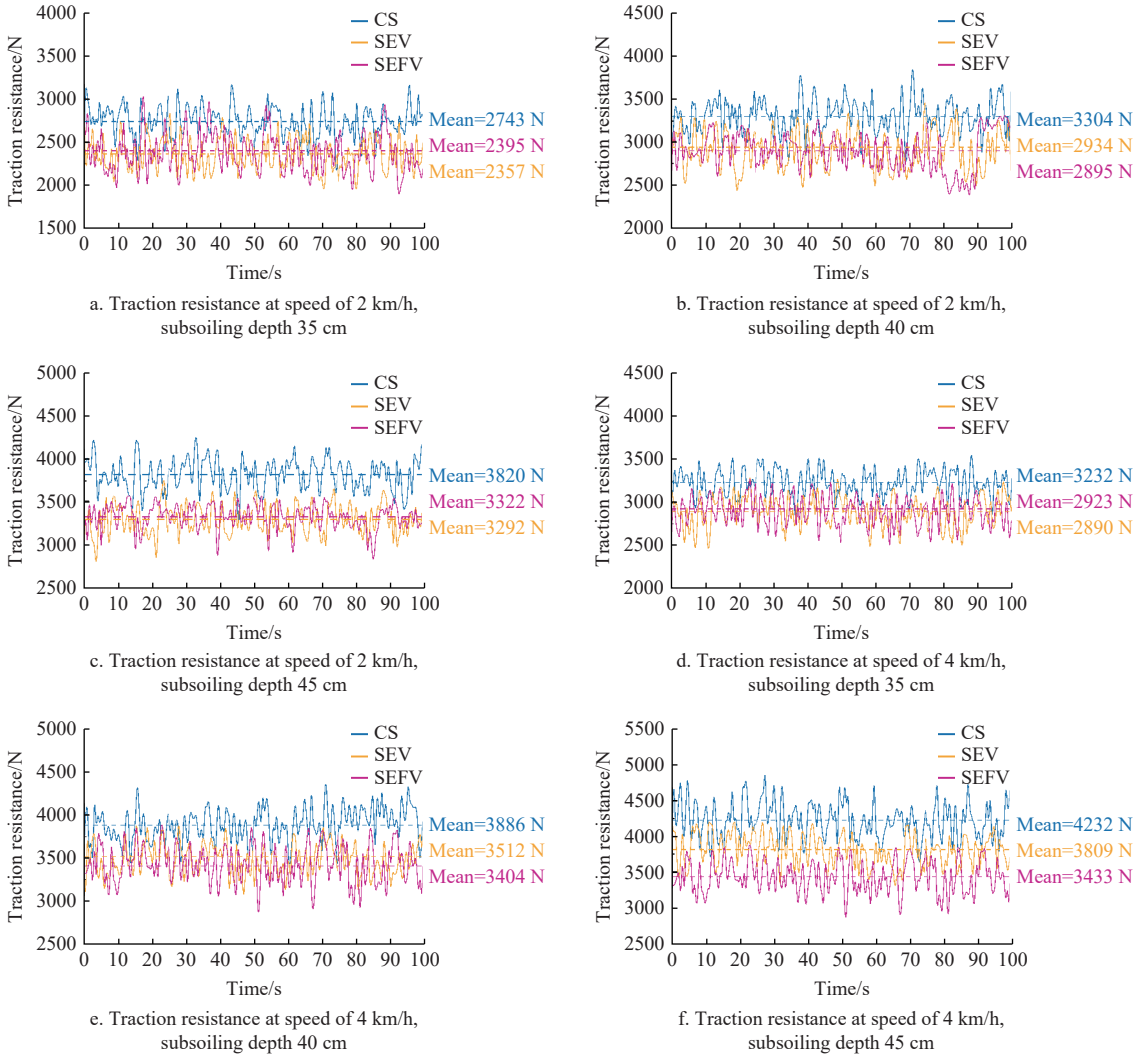

a. Traction resistance at speed of 2 km/h, subsoiling depth 35 cm

b. Traction resistance at speed of 2 km/h, subsoiling depth 40 cm

c. Traction resistance at speed of 2 km/h, subsoiling depth 45 cm

d. Traction resistance at speed of 4 km/h, subsoiling depth 35 cm

e. Traction resistance at speed of 4 km/h, subsoiling depth 40 cm

f. Traction resistance at speed of 4 km/h, subsoiling depth 45 cm

Figure 9 Traction resistance test results

According to the analysis of Figures 9d-9f, when the subsoiler switched to a speed of 4 km/h, the traction resistance of all subsoilers increased significantly. The main reason is that the impact and compressive deformation of the soil intensified, resulting in greater soil resistance to the implement. At the same time, when the forward speed of the subsoiler increased, the reaction force applied by the implement to the soil per unit time increased, thereby leading to an increase in cutting resistance. At a depth of 35 cm, the average traction resistance of CS, SEV, and SEFV was 3232 N, 2890 N, and 2923 N, respectively. At a depth of 40 cm, the average traction resistance of CS, SEV, and SEFV was 3886 N, 3512 N, and 3404 N, respectively. At a depth of 45 cm, the average traction resistance of CS, SEV, and SEFV was 4323 N, 3809 N, and 3433 N, respectively. As the working depth increased, the resistance reduction effect of SEFV also gradually increased. At 35 cm, the working states of SEV and SEFV were the same, both being self-excited subsoiling, and their traction resistance was nearly the same and much lower than the traction resistance of CS. However, at 40 cm, some working states of SEV and SEFV had exceeded 3500 N, and the forced vibration state of SEFV was briefly activated, so the traction resistance of SEFV became lower than that of SEV. But since the forced subsoiling was activated for a short time, the difference was not significant, but the resistance was still significantly lower than CS. At 45 cm, the difference in traction resistance between SEFV and SEV was significant. Since the average traction resistance of CS had reached 4323 N, even with the effect of self-excited vibration, the resistance of SEV was as high as 3809 N. Obviously, at this time, the resistance reduction effect of self-excited vibrating subsoiling had approached its limit, while the resistance reduction effect of SEFV gradually began to become

significant. At this time, the working state of SEFV was mostly forced subsoiling and a small part of self-excited subsoiling, so the resistance reduction effect reached the maximum. In summary, at 4 km/h, there was no significant difference between SEFV and SEV at 35 cm, the resistance was reduced by 3.1% at 40 cm, and the resistance was reduced by 9.9% at 45 cm; compared with CS, SEFV showed strong resistance reduction ability at all depths, and the resistance was reduced by 9.6%, 12.4%, and 18.9% at the three working depths, respectively.

4.2 Subsoiling depth stability

Subsoiling depth stability is a critical indicator of operational quality, reflecting the consistency of tillage depth which directly impacts the effectiveness of breaking the compacted soil layer. Table 4 presents the average depth (a) and stability coefficient (U) for the different treatments.

Table 4 Test results of subsoiling depth stability

Test index		Subsoiling depth 35 cm			Subsoiling depth 40 cm			Subsoiling depth 45 cm		
		CS	SEV	SEFV	CS	SEV	SEFV	CS	SEV	SEFV
Working speed 2 km/h	Average subsoiling depth/cm	34.14	33.45	33.13	41.20	39.05	39.27	44.31	43.67	44.37
	Standard deviation of subsoiling depth/cm	1.35	1.72	1.81	2.73	3.63	3.36	2.47	3.72	3.58
	Coefficient of variation/%	3.95	5.14	5.46	6.63	9.30	8.56	5.57	6.82	8.07
	Stability coefficient/%	96.05	94.86	94.54	93.37	90.70	91.44	94.43	91.48	91.93
Working speed 4 km/h	Average subsoiling depth/cm	34.55	33.72	34.14	39.16	38.31	39.62	46.41	43.57	46.20
	Standard deviation of subsoiling depth/cm	1.72	2.62	2.72	2.84	4.16	3.82	3.78	5.62	4.42
	Coefficient of variation/%	4.98	7.77	7.97	7.25	10.86	9.64	8.14	12.90	9.57
	Stability coefficient/%	95.02	92.23	92.03	92.75	89.14	90.36	91.86	87.10	90.43

At the lower operating speed of 2 km/h, all treatments exhibited high depth stability, with U values consistently exceeding 90.70%. The CS showed the highest stability (U values ranging from 93.37% to 96.05%), providing a stable baseline due to its rigid structure. Both the SEV (U values from 90.70% to 94.86%) and the SEFV (U values from 91.44% to 94.54%) also demonstrated excellent stability, meeting the operational quality standard (>80%). The slightly lower stability coefficients for SEV and SEFV compared to CS might be attributed to the minor depth fluctuations inherent in the vibration process itself, even under low resistance conditions. Importantly, there was no significant difference in stability between SEV and SEFV at this speed across all depths. This aligns with the traction resistance results (Section 4.1), confirming that the soil resistance remained below the 3500 N threshold, and thus the SEFV operated solely in the self-excited mode, mirroring the performance of the SEV.

However, significant differences in stability emerged at the higher operating speed of 4 km/h, particularly as working depth increased. The conventional subsoiler maintained relatively good stability, although a slight decreasing trend was observed as depth increased (U dropping from 95.02% at 35 cm to 91.86% at 45 cm). This suggests that the increased traction resistance at higher speed and depth (as seen in Figure 9) made it marginally more challenging for the rigid implement to maintain perfectly uniform depth. The stability of the self-excited vibrating subsoiler (SEV) showed a marked decline with increasing depth at 4 km/h. While acceptable at 35 cm (U=92.23%), stability dropped at 40 cm (U=89.14%) and became significantly compromised at 45 cm, with the stability coefficient falling to 87.10%. Furthermore, the average working depth achieved by SEV at 45 cm was only 43.57 cm, failing to consistently reach the target depth. This performance degradation is directly linked to the high traction resistance encountered (average 3809 N, Figure 9f). Under such high loads, the effectiveness of the self-excited vibration mechanism is limited, potentially leading to inconsistent vibration amplitude or even vibration failure, resulting in poor depth control and reduced stability. In stark contrast, the SEFV demonstrated consistently high depth stability across all depths at 4 km/h, with U values of 92.03% at 35 cm, 90.36% at 40 cm, and 90.43% at 45 cm. This superior stability, especially compared to SEV at 40 cm and 45 cm depths, highlights the crucial benefit of the adaptive forced vibration mode. As traction resistance increased with depth, exceeding the 3500 N threshold (particularly at 40 cm intermittently and predominantly at 45 cm, as discussed in Section 4.1), the SEFV system automatically engaged its forced vibration component. This active, powered vibration effectively assisted the subsoiler shank in penetrating the high-resistance soil consistently, ensuring stable operation and maintaining the target depth. Notably, at 45 cm depth, the average depth achieved by SEFV was 46.20 cm, slightly exceeding the target, likely due to the enhanced soil shattering effect of the forced vibration, while still maintaining high stability (U=90.43%). The control system's response logic, incorporating the 0.5 s threshold duration for sustained high resistance, demonstrated stable and effective transitions between self-excited and forced vibration modes during the field tests. This approach successfully balanced the need for responsiveness to changing soil conditions with the requirement for operational stability, preventing excessive mode hunting.

In summary, the analysis of subsoiling depth stability clearly demonstrates the advantage of the SEFV's adaptive control strategy. While all methods performed well at lower speeds/resistances, the SEFV significantly outperformed the SEV under challenging conditions (higher speed and deeper tillage) by maintaining high depth stability through the timely intervention of forced vibration. This ability to adapt its working mode ensures consistent operational quality across a wider range of soil resistance levels, addressing a key limitation of purely self-excited systems and validating the design rationale of the intelligent vibrating subsoiler.

5 Conclusions

1) A novel self-excited and forced intelligent vibrating subsoiler (SEFV) featuring an adaptive control mechanism was successfully designed and developed. The system automatically switches between self-excited and forced vibration modes based on real-time soil resistance feedback.

2) Field experiments confirmed the effectiveness of the adaptive strategy. Under low resistance conditions, the SEFV operated efficiently in self-excited mode, matching the performance of a purely self-excited system (SEV) while significantly reducing resistance compared to conventional subsoiling (CS). Crucially, under high resistance conditions where SEV performance degraded,

the SEFV automatically engaged forced vibration, achieving superior traction resistance reduction compared to both SEV and CS.

3) The SEFV demonstrated robust performance by maintaining high subsoiling depth stability (>90%) across all tested conditions. The intelligent adaptive control allows the subsoiler to maintain operational effectiveness (both resistance reduction and depth stability) across variable soil resistance levels, offering a promising approach for energy-efficient farming, particularly in challenging high-resistance soil conditions, by optimizing vibration mode usage.

4) While this study demonstrated promising results in the tested black soil, further research and validation are necessary to evaluate the performance and adaptability of the SEFV technology across a wider range of soil types and conditions to fully assess its broader applicability.

Acknowledgements

This work is supported by the National Key Research and Development Program of China (Grant No. 2024YFD2000100), the National Natural Science Foundation of China (Grant No. 52105300 and 52075215), and the Science and Technology Research Project of Jilin Provincial Education Department (Grant No. JJKH20250136KJ).

[References]

[1] Ning T Y, Liu Z, Hu H Y, Li G, Kuzyakov Y. Physical, chemical and biological subsoiling for sustainable agriculture. Soil and Tillage Research, 2022; 223: 105490.

[2] Wang S B, Guo L L, Zhou P C, Wang X J, Shen Y, Han H F, Ning T Y, Han K. Effect of subsoiling depth on soil physical properties and summer maize (*Zea mays* L.) yield. Plant, Soil & Environment, 2019; 65(3): 131–137.

[3] Wang Y X, Chen S P, Zhang D X, Yang L, Cui T, Jing H R, et al. Effects of subsoiling depth, period interval and combined tillage practice on soil properties and yield in the Huang-Huai-Hai Plain, China. Journal of Integrative Agriculture, 2020; 19(6): 1596–1608.

[4] Wang Y M, Li N, Ma Y H, Tong J, Pfleging W, Sun J Y. Field experiments evaluating a biomimetic shark-inspired (BioS) subsoiler for tillage resistance reduction. Soil and Tillage Research, 2020; 196: 104432.

[5] Yuan J, Yu J Q. Analysis on operational process of self-excited vibrating subsoiler based on DEM-MBD coupling algorithm. Transactions of the CSAM, 2020; 51(S1): 17–24. (in Chinese)

[6] Ma X, Wang S J. Design and study on vibration characteristics of self-excited vibration layered subsoiler for coastal soil. Journal of Coastal Research, 2020; 103(SI): 318–322. 10.2112/SI103-066.1

[7] Zhou H, Zhang W L, Yang Q J, Li D D, Xia J F. Design and experiment of sliding cutting self-excited vibration drag reduction subsoiling device. Transactions of the CSAM, 2019; 50(5): 71–78. (in Chinese)

[8] Sun Y P, Dong X Q, Song J N, Wang J C, Liu C L, Xu G H. Self-balancing performance and simulation analysis of multi-group vibrating sholvels of oscillatory subsoiler. Transactions of the CSAE, 2018; 34(4): 92–99. (in Chinese)

[9] Sun Y, P Dong X Q, Song J N, Liu C L, Wamg J C, Zhang C. Parameter optimization of vibration subsoiler test bed for reducing resistance and vibration. Transactions of the CSAE, 2016; 32(24): 43–49. (in Chinese)

[10] Zhang J C, Yan X L, Lin Z K, Zhu R X. Design and experiment of self-exciting vibration deep-loosening and sub-soiling machine. Transactions of the CSAM, 2016; 47(9): 44–49,72. (in Chinese)

[11] Wang Y X, Jing H R, Zhang D Z, Cui T, Zhong X J, Yang L. Development and performance evaluation of an electric-hydraulic control system for subsoiler with flexible tines. Computers and Electronics in Agriculture, 2018; 151: 249–257.

[12] Wang Y, Zhang D, Yang L, Cui T, Zhang W, Qi B, Li Y, Zhong X. Field performance of an electric–hydraulic control system for vibrating subsoiler with flexible tines. Computers and electronics in agriculture, 2020; 172: 105377.

[13] Cui T, Shi Z D, Yang L, Wang Y X, Han D D, Zhang D X. Design and experiment of vibration subsoiler with adjustable spring pre-tightening force. Transactions of the CSAM, 2016; 47(S1): 96–102. (in Chinese)

[14] Zhang X R, Wang C, Chen Z H, Zeng Z W. Design and experiment of a bionic vibratory subsoiler for banana fields in southern China. Int J Agric & Biol Eng, 2016; 9(6): 75–83.

[15] Wang Y X, Osman A N, Zhang D X, Yang L, Cui T, Zhong X J. Optimized design and field experiment of a staggered vibrating subsoiler for conservation tillage. Int J Agric & Biol Eng, 2019; 12(1): 59–65.

[16] Dong X Q, Su C, Zheng H N, Han R Q, Li Y L, Wan L P C, et al. Analysis of soil disturbance process by vibrating subsoiling based on DEM-MBD coupling algorithm. Transactions of the CSAE, 2022; 38(1): 34–43. (in Chinese)

[17] Wang D W, Wang J S, Shang S Q. Experimental research on soil digging resistance and energy consumption based on vibration. Transactions of the CSAM, 2020; 51: 267–272. (in Chinese)

[18] Adamchuk V I, Ingram T J, Sudduth K A, Chung S O. On-the-go mapping of soil mechanical resistance using a linear depth effect model. Transactions of the ASABE, 2008; 51(6): 1885–1894.

[19] Zhou D Y, Hou P F, Xin Y L, Wu B G, Tong J, Yu H Y, et al. Resistance and consumption reduction mechanism of bionic vibration and verification of field subsoiling experiment. Applied Sciences, 2021; 11(21): 10480.

[20] Baran R, Michalczyk K, Warzecha M. Experimental analysis of transverse stiffness distribution of helical compression springs. Acta Mechanica Et Automatica, 2023; 17(1): 95–103.

[21] Taktak M, Omheni K, Aloui A, Dammak F, Haddar M. Dynamic optimization design of a cylindrical helical spring. Applied Acoustics, 2014; 77: 178–183.

[22] Ali M, Nazir A, Jeng J Y. Mechanical performance of additive manufactured shoe midsole designed using variable-dimension helical springs. The International Journal of Advanced Manufacturing Technology, 2020; 111: 3273–3292.

[23] Lin Y L, Yang T T, Guo Y Q, Chen S, Li J B. Study on hybrid test control system based on MATLAB-STM32. Instruments and Experimental Techniques, 2022; 65(2): 218–231.

[24] Zhang Y Q, Tang Y C, He D, Shi J, Hao L R, Li J B, et al. Design and test of electromagnetic vibration type fine and small-amount seeder for millet. Agriculture, 2024; 14(9): 1528.